A New Noise-Suppression Algorithm for Transient Thermal Analysis in Semiconductors Over Pulse Superposition

Maximilian Schmid, Sri Krishna Bhogaraju, Alexander Hanss, and Gordon Elger

***Abstract*— This article introduces a new measurement method for noise suppression in transient thermal analysis (TTA), which is used to measure the transient thermal impedance of power semiconductors and LEDs. An additional short pulse sequence is added to the standard TTA measurement procedure. The thermal response of this additional sequence is converted into the original single-pulse response of standard TTA by superposition of previous pulses in the sequence. Applying this method, the noise before 1 ms can be significantly reduced without averaging over multiple measurement repetitions that would increase the measurement time accordingly. The noise reduction for times below 1 ms is important to resolve the thermal resistance layers close to the junction of a semiconductor. The measurement method and data analysis algorithm are developed for TTA measurements, but the principle is suitable for all linear time-invariant (LTI) systems where the system response is measured over several time decades. The algorithm was evaluated on simulated and experimental data of a power LED. With an additional sequence of only 100 ms, a signal-to-noise ratio (SNR) improvement of 15.1 dB for simulated data and 14.7 dB for experimental data was achieved. This is equivalent to averaging over 30 repetitions in the standard TTA procedure. Therefore, the new method achieves a reduction of measurement time of 97% for applications where low noise levels are required for times below 1 ms.**

***Index Terms*— LED, linear time-invariant (LTI) system, MOSFET, noise suppression, reliability, semiconductor, signal processing, thermal impedance (Z_{th}), transient thermal analysis (TTA).**

I. Introduction

THE power electronic market will grow further in the next years, especially under the drive of the automotive and renewable energy sectors. High reliability is required in most of the applications since failures are safety relevant or costly in maintenance or replacement. One of the most crucial components in power electronics are semiconductors, which are responsible for nearly a fourth of the failures [1], caused primarily by high temperature and high current. Driven by the increasing power density due to miniaturization and the new wideband technologies, the importance of these failures will increase in the next years [2] and thermal reliability analyses will be a key aspect for power semiconductors in the future.

Different evaluation methods are used to qualify the thermal integrity of semiconductors. Most common in production is X-ray inspection to detect voids and nonwetted areas in the solder layer. However, for sintering—an interconnection technology of increasing importance for high-temperature applications—X-ray is not suitable since the porosity in sintered interconnects is too small for the resolution of the X-ray images. An alternative is acoustic microscopy (SAM), but here the module must be placed under water and manufacturers want to avoid the drying process. In addition, multiple reflection layers and the thin interface heights often impede the evaluation of SAM images. A third method is transient thermal analysis (TTA) that allows the evaluation of the thermal response of a semiconductor according to internal power losses during usage. TTA permits observing the thermal path from the junction to the heat sink and identifies the contribution of single physical layers in between. One challenge for TTA is the signal-to-noise ratio (SNR) for times below 1 ms, which is required to resolve the layers in the thermal path close to the junction. A high SNR is necessary to evaluate information in this time range for curve fitting [3], [4] and for computing the thermal structure function (STF) [5], [6]. Since high bandwidth is required in this time range, analog or digital low-pass filtering is not possible without information loss. Noise suppression is only possible through averaging over multiple measurement repetitions, which is very time consuming since the thermal equilibrium of the analyzed system must be reached before every repetition. Depending on the thermal setup, this can take from seconds to minutes. To reduce the time needed for noise suppression, a new pulse sequence with appropriate data processing algorithm is developed to allow averaging of the measurement signal for times below 1 ms without reaching thermal equilibrium. Thus, the time requirement is strongly reduced by only adding a short pulse sequence to the standard procedure. The work in this article is an extended version of the conference publication [7]. Although this article focuses on TTA, the approach of the method and the algorithm is in general applicable on linear time-invariant (LTI) systems, where it is required to measure over several time decades to determine the full system response and the SNR for the first decades is essential for system identification.

Manuscript received March 23, 2020; accepted July 16, 2020. Date of publication July 24, 2020; date of current version December 1, 2020. This work was supported by the Bavarian Ministry of Science and Art under Project PTTA (H.2-F1116.IN/25/3). The Associate Editor coordinating the review process was Dong Wang. *(Corresponding author: Maximilian Schmid.)*

The authors are with the Institute of Innovative Mobility (IIMo), Technische Hochschule Ingolstadt, 85049 Ingolstadt, Germany (e-mail: maximilian.schmid@thi.de; srikrishna.bhogaraju@thi.de; gordon.elger@thi.de; alexander.hanss@thi.de).

Digital Object Identifier 10.1109/TIM.2020.3011818

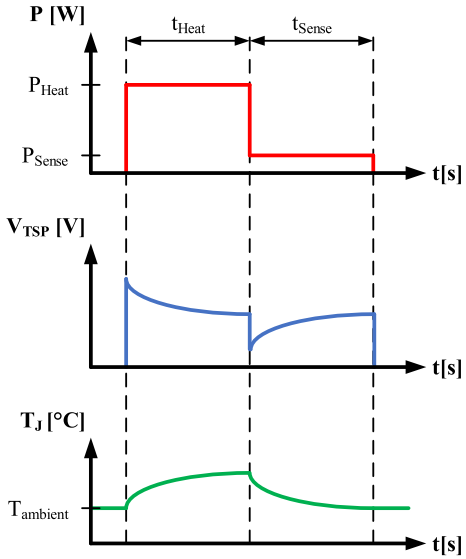

Fig. 1. Procedure for standard TTA.

II. Transient Thermal Analysis

A. Measurement Principle of Standard TTA

The investigated parameter for TTA is the thermal impedance $Z_{\text{th}}(t)$, representing the time-resolved temperature change according to a single power step P

$$Z_{\text{th}}(t) = \frac{\Delta T(t)}{P}. \tag{1}$$

The measurement procedure is defined in [8] and refined for different semiconductor types in [9]–[13]. At first, the semiconductor is driven in a nominal condition, resulting in a thermal loss (P_{Heat}) that heats up the semiconductor. After the thermal equilibrium is reached, P_{Heat} is switched OFF and only a small sensing power (P_{Sense}) is applied, causing the semiconductor to cool down. Thermal equilibrium has to be reached first, so only a single pulse (power step when switching from P_{Heat} to P_{Sense}) causes the response of the thermal system. During t_{Sense}, the junction temperature $T_j(t)$ of the semiconductor is measured by a temperature-sensitive electrical parameter (TSP) and $Z_{\text{th}}(t)$ is computed with (1). The whole sequence is schematically shown in Fig. 1.

The electrical realization of applying P_{Heat} and P_{Sense} in which TSP is used depends on the semiconductor type and can differ (e.g., forward voltage for heating and sensing of diodes or heating over channel and sensing by $V_{\text{GS-th}}$ for MOSFETs [14]). However, the measurement principle is always the same.

B. Structure and Bandwidth of $Z_{th}(t)$

The thermal path from junction to heat sink defines the signal shape of $Z_{\text{th}}(t)$ and is physically described by a Cauer network (see Fig. 2(a)). The path is therefore separated in multiple small layers. Each layer consists of a thermal capacity $C_{\text{th}-i}$ and a thermal resistance $R_{\text{th}-i}$ according to its material properties and dimensions. For mathematical analysis, the Cauer network is transformed into a Foster network (see Fig. 2(b)), where the capacities $C'_{\text{th}-i}$ are in parallel to the

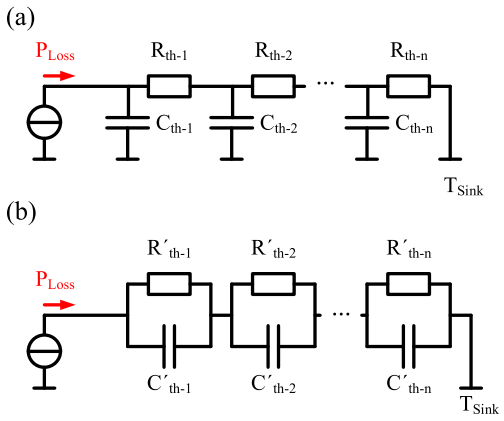

Fig. 2. Thermal networks in (a) Cauer type and (b) Foster type.

resistances $R'_{\text{th}-i}$. Note that the transformed values $C'_{\text{th}-i}$ and $R'_{\text{th}-i}$ no longer represent the physical capacitance and resistance. The mathematical description of $Z_{\text{th}}(t)$ with the Foster network is much simpler [15]

$$Z_{\text{th}}(t) = \sum_{i=1}^{n} R'_{\text{th}-i}\left(1 - e^{-\frac{t}{\tau_i}}\right) \tag{2}$$

with:

$$\tau_i = C'_{\text{th}-i} * R'_{\text{th}-i}. \tag{3}$$

$Z_{\text{th}}(t)$ consists of a sum of exponential functions starting at the same time $t_0 = 0$, i.e., when the thermal power step P occurs. To determine potential low-pass filtering for noise reduction, the bandwidth of the thermal response is evaluated by calculating the frequency spectrum of a single RC node, i.e., single thermal resistance layer, using the one-sided Fourier transformation (see (4)) for causal signals [16]. The one-sided Fourier transformation was chosen since $Z_{\text{th}}(t) = 0$ for $t < 0$. Only the exponential term of (2) was considered in (4) because the constant term is represented by a Dirac impulse at 0 Hz in the frequency domain and has no influence on the bandwidth

$$|S(f)| = R'_{\text{th}-i}/\sqrt{(1/\tau_i)^2 + 4\pi^2 * f^2}. \tag{4}$$

Defining that an RC node has no significant influence on $Z_{\text{th}}(t)$ after 5τ since it already reached 99.3% of its final value and additionally defining the cutoff frequency f_c to -3 dB, then the time dependence of f_c is given by (5). The bandwidth B is defined from 0 Hz to f_c and is inversely decreasing over the time (see Fig. 3)

$$f_c(t) = B(t) = \frac{1}{2\pi * t/5}. \tag{5}$$

$B(t)$ decreases by a factor 10 per time decade. At 1 μs, the useful signal, i.e., the spectrum calculated from $t = 1$ μs until $t \to \infty$, has a bandwidth of 800 kHz, which decreases to only 0.8 kHz at 1 ms, i.e., spectrum calculated from $t = 1$ ms until $t \to \infty$ since only lower frequent RC nodes, i.e., large τ_i, are influencing the signal at this time. Therefore, measurement noise overlapping the useful signal can be reduced much more by a digital low-pass filter in a later time range compared to an earlier one since a lower cutoff frequency for the low pass

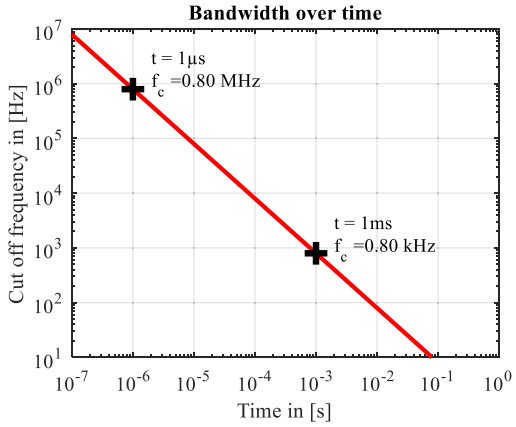

Fig. 3. Bandwidth of $Z_{\text{th}}(t)$ over time.

can be selected without an information loss. Conversely, it is more difficult to achieve high SNR at early times of $Z_{\text{th}}(t)$ since the remaining noise is higher.

C. Influence of RC Nodes Close to the Junction on $Z_{th}(t)$

To evaluate the influence of *RC* nodes close to the junction on $Z_{\text{th}}(t)$, a thermal finite-element model (FEM) in FloEFD was set up and optimized to fit the thermal properties of an LED (Type LUXEON F PLUS), soldered onto an Al-IMS-PCB (aluminum insulated metal substrate) and mounted with a thermal interface material to a heat sink. A detailed description of the model and its calibration and optimization can be found in [17]. Three transient thermal simulations were performed using the model, one with the optimized settings and two with 66% and 33% decreased thermal conductivity of the layer closest to the junction (the epitaxial passivation layer–1 μm thickness) to ensure an early separation. The results of the simulations are shown in Fig. 4(a) for $Z_{\text{th}}(t)$ and their difference to the optimized setting in Fig. 4(b). The curves start separating at approximately 3 μs and a final difference of 0.16–0.64 K/W is reached. To observe these early changes in $Z_{\text{th}}(t)$ and detect this failure mode, a high SNR in this time range is necessary.

D. Influence of Noise on TTA Data Evaluation

Evaluation of TTA data can be done in different ways. The simplest method is comparing the thermal resistance R_{th} (i.e., $Z_{\text{th}}(t)$ for $t \to \infty$) between different devices. Alternatively, the signal shape of $Z_{\text{th}}(t)$ can be compared to find the point of separation where the thermal paths start to differ (as done in Fig. 4). There are also more complex evaluation methods such as the normalized logarithmic derivative or the structure function. For all evaluation methods, different mathematical transformations are needed. A summary describing the data processing is shown in Fig. 5. The influence of noise on the mathematical transformations is discussed in detail in the following.

1) Z_{th}/R_{th} Evaluation: The first required algorithm is an extrapolation of the early time data of the measured $Z_{\text{th}}(t)$. Due to electrical responses and disturbances while switching from P_{Heat} to P_{Sense}, the measured signal is incorrect before

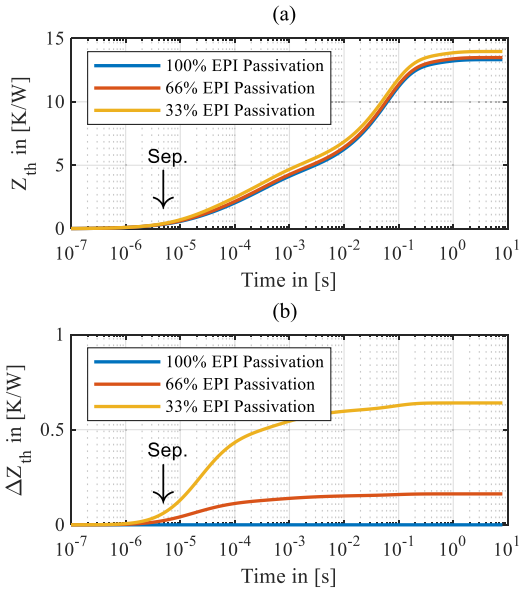

Fig. 4. Separation of $Z_{\text{th}}(t)$ in the early time range. (a) Comparison of $Z_{\text{th}}(t)$. (b) Difference in $Z_{\text{th}}(t)$ to 100% EPI passivation.

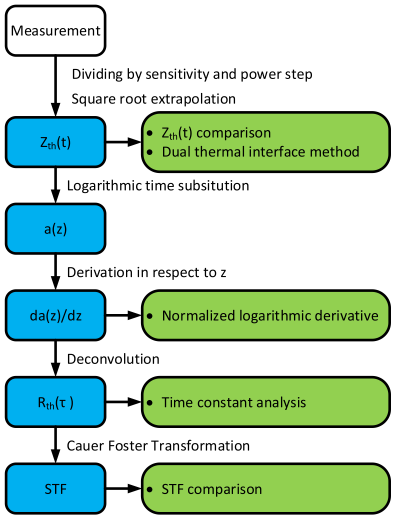

Fig. 5. Evaluation methods for TTA with mathematical transformations.

a setup-dependent time has passed. An extrapolation is necessary to get information at $t = 0$ s and adjust $Z_{\text{th}}(0\text{ s})$ to 0 K/W. Typically, a linear relation of the data to the square root of the time is used for extrapolation. This represents the theoretical behavior of a semi-infinite plate of homogeneous material for 1-D heat flow vertical to the surface [18]. The susceptibility of the square root extrapolation (SQRT-Ex) to noise was analyzed with the same FEM model from Section II-C. A transient thermal simulation was performed with 1-μs time steps until 1 ms to generate $Z_{\text{th}}(t)$. White noise with different quadratic means $\text{rms}_{\text{noise}}$ was added to the simulated $Z_{\text{th}}(t)$ via a random process to obtain SNRs of 40–70 dB matched to the signal amplitude ($R_{\text{th}} = 13.3$ K/W) of the model following (6). White noise was selected because it is very similar to the experimental determined noise behavior of our measurement equipment

$$\text{SNR} = 20\log(R_{\text{th}}/\text{rms}_{\text{noise}}). \tag{6}$$

TABLE I
VARIANCE OF ERROR FOR SQRT-EXTRAPOLATION IN K/W AND RELATIVE TO R_{th} ACCORDING TO DIFFERENT SNRS

	Extrapolation time interval	
SNR	1 µs … 10 µs	20 µs … 40 µs
40 dB	0.143 K/W (1.073 %)	0.282 K/W (2.12 %)
50 dB	0.046 K/W (0.346 %)	0.089 K/W (0.667 %)
60 dB	0.015 K/W (0.113 %)	0.028 K/W (0.212 %)
70 dB	0.005 K/W (0.034 %)	0.009 K/W (0.068 %)
no Noise	0 K/W (0 %)	0 K/W (0 %)

TABLE II
PEAK VARIANCE OF NORMALIZED LOGARITHMIC DERIVATIVE ACCORDING TO NOISE

	Normalization time interval	
SNR	40 µs … 200 µs	40 µs … 500 µs
40 dB	10.115 %	6.923 %
50 dB	2.958 %	1.911 %
60 dB	0.917 %	0.632 %
70 dB	0.298 %	0.205 %
no Noise	0 %	0 %

Two SQRT-Ex with different time intervals as fit region were applied to the noisy data: one for an early (1–10 μs) and one for a later time interval (20–40 μs). The variances of the SQRT-Ex for $Z_{th}(0\ s)$ over 1000 runs for each SNR level and fit region are listed in Table I and is observed to be decreasing with rising SNR. The early fit region is thereby less susceptible since a smaller time range has to be bypassed to 0 s, even if more samples are used for the later extrapolation. At 40 dB, a variance of 2.12% of the complete R_{th} was computed. Compared to the common failure criterion of 20% R_{th} increase while aging, this influence cannot be neglected and a high SNR is necessary for an accurate zero-time extrapolation.

2) Normalized Logarithmic Derivative: The SQRT extrapolated $Z_{th}(t)$ is converted into $a(z)$ by the substitution $z = \ln(t)$. Within this processing step, a resampling of data points from a linear to a logarithmic equidistant time scale is performed by linear interpolation. For this article, an advanced resampling algorithm is used, with additional noise reduction by 10 dB per decade starting from 1 ms by averaging a number of samples. Afterward, a filter can be used to smoothen the data without affecting the spectrum of the useful signal before computing the derivation of $a(z)$ with respect to z.

The logarithm of the derivative $da(z)/dz$ is used for the second evaluation method. The logarithmic derivative is thereby normalized at a certain time interval. In this way, it is not necessary to know TSP and power step since with the normalization they are transferred into an axis offset, and hence, a time-intensive characterization is not needed. The normalization is done in a time range much smaller than 1 ms, where the thermal response is only influenced by the material and package properties of the measured component and not by its interconnect and the substrate. The data can be normalized, assuming that material and package properties are similar due to low semiconductor manufacturing variances. The investigated parameter is the relative change in maximum peak. A higher peak means a poorer thermal path and an increase of 5% is considered as fail. A detailed description of the normalized logarithmic derivative method can be found in [5].

To investigate the susceptibility to noise, the thermal model from Section II-C was used. The data were generated in logarithmic equidistant time steps, and white noise was added to obtain SNR levels from 40 to 70 dB, each with a noise reduction of 10 dB per decade starting from 1 ms. The derivative was calculated for 1000 data sets for one SNR level and normalized in two time intervals (40–200 μs and 40–500 μs). The variance of the peaks in percentage is listed in Table II. With an SNR of only 40 dB, this method is not able to yield useful results. The variance due to noise is 10.1% in the early and 6.9% in the later normalization interval, both of which are higher than the error limit. The impact of noise becomes negligible once 60 dB SNR is reached. The variance is reduced using a longer normalization interval. However, longer intervals increase the chance of separation inside the normalization interval and therefore cause invalidity of the normalization. Overall, this evaluation is much more sensitive to noise and needs a high SNR of at least 60 dB.

3) $R_{th}(\tau)$/Structure Function: The third analyzed evaluation method also starts with the derivative $da(z)/dz$, but instead of using the logarithmic form, the spectrum $R_{th}(\tau)$ of $Z_{th}(t)$ is calculated by a deconvolution. From $R_{th}(\tau)$, the widely used structure function (STF) is calculated by a Foster–Cauer transformation [19]. For evaluation of the influence of noise, noise was added identical to Section II-D2 and a Bayesian deconvolution with 1000 iteration was used [20] to compute $R_{th}(\tau)$. The rating of the similarity of computed $R_{th}(\tau)$ to the noiseless reference is done by the correlation coefficients (CCs) by cross correlation. In Fig. 6, one generic spectrum for each SNR level is shown, and Table III lists the average CC over 1000 calculations per SNR level. With 50-dB SNR, a similarity of only 76.4% was reached. The spectra differ strongly for τ smaller than 10 ms, which can be seen in Fig. 6 by comparing the blue (50 dB) and the purple line (no noise). For 60 dB SNR (red line), a similarity of 99.0% was reached, but even here peaks for small τ can be observed.

From the three analyzed evaluation methods, the $R_{th}(\tau)$/structure function is most susceptible to noise, but all need an SNR of approximately 60 dB to provide reliable data. This level is difficult to reach without multiple measurement repetitions. To avoid the large extra time, a time-saving noise suppressing algorithm for better data evaluation is needed.

III. DETERMINISTIC PULSE ALGORITHM

A. Introduction of the Algorithm

The new deterministic pulse algorithm (DPA) is aiming to reduce the noise for times before 1 ms. Only a short DPA sequence is added before the standard TTA sequence

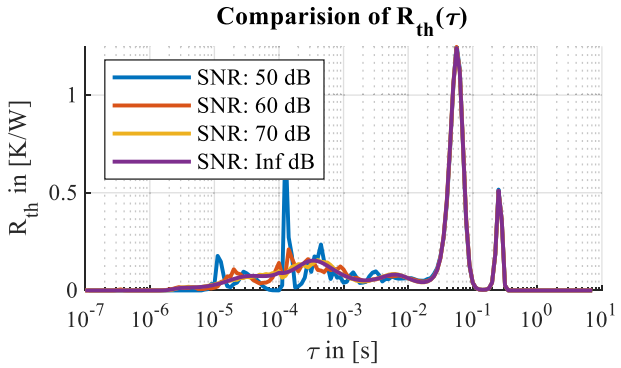

Fig. 6. Comparison of $R_{\mathrm{th}}(\tau)$ spectrum for different SNR levels [$R_{\mathrm{th}}(\tau)$ for 40 dB was removed for optical clearness].

TABLE III
RATING OF SIMILARITY OF SPECTRUM BY CC ACCORDING TO SNR

SNR	40 dB	50 dB	60 dB	70 dB	no Noise
CC	53.2 %	76.4 %	99.0 %	99.9 %	100 %

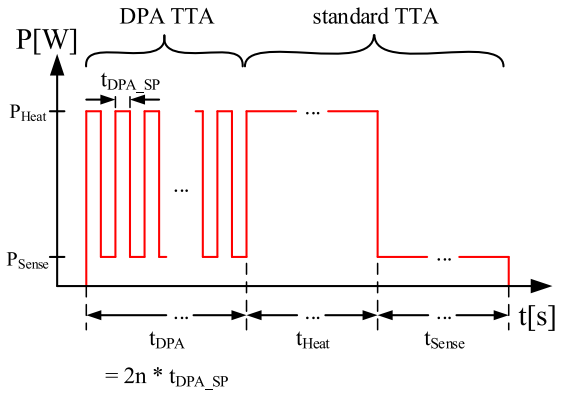

Fig. 7. Pulse sequence of DPA.

and the complete sequence is shown in Fig. 7. Overall, n short heat phases and n short sense phases all with the same single phaselength $t_{\mathrm{DPA\_SP}}$ are additionally applied to the semiconductor, where $t_{\mathrm{DPA\_SP}}$ is much shorter than t_{Heat} and t_{Sense}. The complete sequence is only extended by the time t_{DPA} ($=2n^{*}t_{\mathrm{DPA\_SP}}$) and thermal equilibrium is never reached during t_{DPA}, which is also not necessary (definition for this article: a pulse is defined as a change in thermal power loss at a certain time. A phase, such as t_{Sense} and $t_{\mathrm{DPA\_SP}}$, is defined as a time phase where a constant power is applied to the semiconductor).

For noise suppression, the DPA averages over all sense phases in t_{DPA} while the temperature of the semiconductor is measured during the sense phases identical to standard TTA. However, these temperature responses are all different and also cannot be directly converted into $Z_{\mathrm{th}}(t)$ with (1) since the definition of $Z_{\mathrm{th}}(t)$ is based on a single-pulse response. For standard TTA, this is possible because the thermal equilibrium is reached during t_{Heat} and only the negative pulse form P_{Heat} to P_{Sense} affects the response. During t_{DPA}, the single-pulse response of any single pulse is overlapped by the responses to all previous pulses according to the pulse superposition principle in (7), where n is the total number of pulses, ΔP_i is the change in power for one pulse, and t_i is the time when this pulse occurred [21]

$$\Delta T(t) = \sum_{i=0}^{n} \Delta P_i * Z_{\mathrm{th}}(t - t_i). \tag{7}$$

Therefore, the single-pulse responses have to be calculated from the measured responses with (7) before averaging. The principle is visualized in Fig. 8. There are three heat phases ($P_{\mathrm{Heat}} = 3$ W) and two sense phases ($P_{\mathrm{Sense}} = 0$ W, i.e., very small compared to P_{Heat}) resulting in five pulses. Three of them are positive pulses (start of heat phase) with even indices, and two of them are negative pulses (start of sense phase) with odd indices. All pulses have the same amplitude $P = P_{\mathrm{Heat}} - P_{\mathrm{Sense}}$ with alternating signs, and the length of phases $t_{\mathrm{DPA\_SP}}$ was set to 1 ms. To compute single-pulse responses (red lines) from the measured responses (black line), a temperature offset $T_{\mathrm{Off}-i}(t)$ has to be subtracted. These offsets are marked as striped gray and white areas in Fig. 8 and are different for every sense phase in t_{DPA}. The temperature offsets can be calculated by addition of all existing gray lines (responses to earlier pulses) in the phase. Specifically, this is done for $T_{\mathrm{Off}-1}(t)$ in (8) and for $T_{\mathrm{Off}-2}(t)$ in (9). For $T_{\mathrm{Off}-1}(t)$, only the response of Pulse_0 is used since it is the only previous pulse. The temperature offset is calculated with (1), where $Z_{\mathrm{th}}(t)$ is shifted by 1 ms because Pulse_0 occurs $1^{*}t_{\mathrm{DPA\_SP}} = 1$ ms earlier than the current Pulse_1. For $T_{\mathrm{Off}-2}(t)$, two earlier pulses have to be considered with identical power step ΔP for both pulses. In general, $T_{\mathrm{Off}-i}(t)$ can be calculated with (10), which is derived from (7) using the superposition principle for input pulses generally valid for LTI systems

$$T_{\mathrm{Off}-1}(t) = \Delta P * Z_{\mathrm{th}}(t + 1\ \mathrm{ms}) \tag{8}$$

$$T_{\mathrm{Off}-2}(t) = \Delta P * (Z_{\mathrm{th}}(t + 2\ \mathrm{ms}) - Z_{\mathrm{th}}(t + 1\ \mathrm{ms})) \tag{9}$$

$$T_{\mathrm{Off}-i}(t) = \Delta P * \sum_{m=1}^{i} (-1)^m * Z_{\mathrm{th}}(t + m * 1\ \mathrm{ms}). \tag{10}$$

For the $T_{\mathrm{Off}-i}(t)$ calculation, only parts of $Z_{\mathrm{th}}(t)$ with $t > t_{\mathrm{DPA\_SP}}$ are required, which are obtained by the standard TTA measurement. Since these parts are in the time range $>$ 1 ms, it is possible to strongly suppress measurement noise by a low-pass filter without changing the time response of the signal. Due to the filtering, the offsets $T_{\mathrm{Off}-i}(t)$ have a low SNR, which is required for the noise suppression in DPA.

The single-pulse responses $Z_{\mathrm{th}-i}(t)$ are calculated with the measured responses $T_i(t)$ and the offsets $T_{\mathrm{Off}-i}(t)$ for every phase i in t_{DPA} with (11). The equation applies for $t \in [0; t_{\mathrm{DPA\_SP}}]$. All $2^{*}n$ computed $Z_{\mathrm{th}-i}(t)$ can be used for averaging $Z_{\mathrm{th}}(t)$ to suppress the noise. In application, only the $Z_{\mathrm{th}-i}(t)$ from the sense phases (odd indices) are used since voltage–temperature measurement are more accurate during low current sense phases

$$Z_{\mathrm{th}-i}(t) = \frac{T_i(t) - T_{\mathrm{Off}-i}(t)}{(-1)^i * \Delta P_i}. \tag{11}$$

Finally, $Z_{\mathrm{th}}(t)$ for $t < t_{\mathrm{DPA\_SP}}$ from the DPA and $Z_{\mathrm{th}}(t)$ for $t > t_{\mathrm{DPA\_SP}}$ from the standard TTA are fitted together. SNR is increased by averaging of many DPA pulses for times $<$ 1 ms and by low-pass filtering for times $>$ 1 ms.

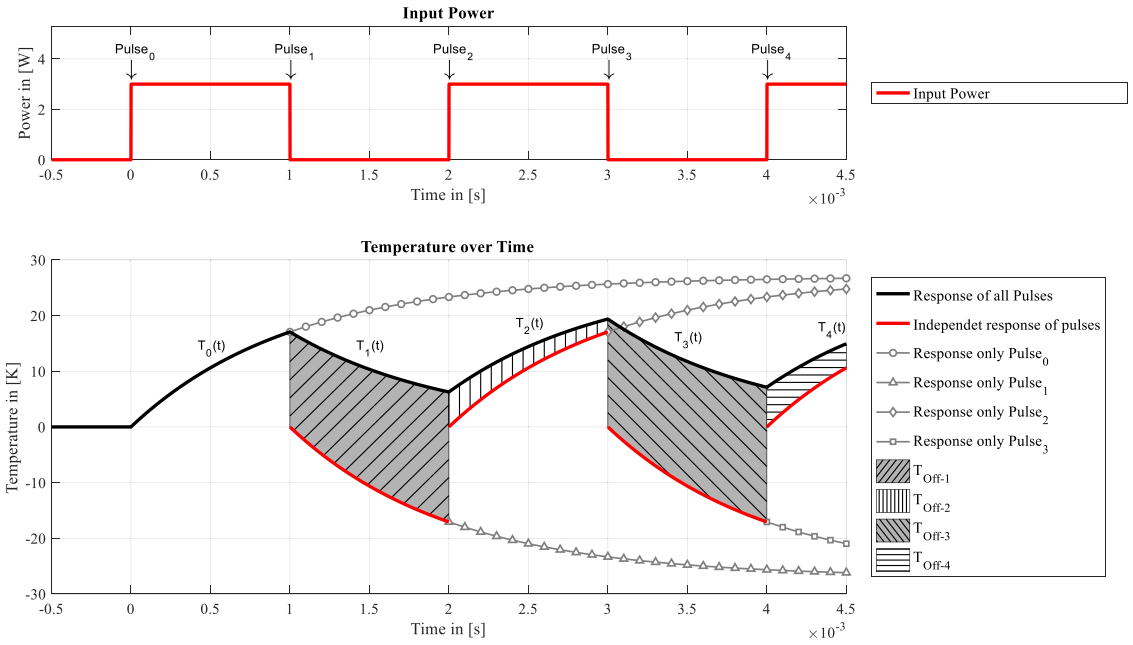

Fig. 8. Superposition principle of pulses for DPA. The black line represents the measured temperature response of the semiconductor for the shown pulse sequence and is separated in single segments according to the different phases and named according to the latest pulse (e.g., $T_0(t)$ from 0 to 1 ms). The red lines (solid and dotted) represent the single-pulse responses to a single pulse for times smaller than $t_{\mathrm{DPA\_SP}}$. The gray lines with different marks show the further progress of these single-pulse responses for $t > t_{\mathrm{DPA\_SP}}$.

B. Theoretical Limit of the Algorithm

For averaging over n standard TTA repetitions, the noise reduction is proportional to $1/\sqrt{n}$ and therefore unbounded [22]. For DPA, this is different and the maximal noise reduction depends strongly on the measurement noise of the calculated temperature offsets $T_{\mathrm{Off}-i}(t)$. All $T_{\mathrm{Off}-i}(t)$ are calculated as a sum of parts of $Z_{\mathrm{th}}(t)$ for $t > t_{\mathrm{DPA\_SP}}$ and with higher i more terms have to be considered. In addition, the noise is not uncorrelated since, e.g., $Z_{\mathrm{th}}(t)$ for $t_{\mathrm{DPA\_SP}} < t < 2^{*}t_{\mathrm{DPA\_SP}}$ has to be used for computation of every $T_{\mathrm{Off}-i}(t)$. The noise on these parts is reduced by a low-pass filter, but it is still present with smaller amplitude.

To evaluate the noise reduction by DPA, we assume that the noise is reduced due to filtering by a factor R for all parts in $Z_{\mathrm{th}}(t)$ for $t > t_{\mathrm{DPA\_SP}}$. Then, noise reduction for n DPA pulses can be expressed with (12) consisting of two terms in the radix of a square root.

$$\mathrm{Reduction}(n) = \sqrt{\frac{1}{n} + R * \left(\frac{\sum_{i=2}^{n} 2 * (i)^2}{n^2} - 1\right)}. \quad (12)$$

The first term $(1/n)$ represents the noise of the DPA response. The second term represents the noise of $T_{\mathrm{Off}-i}(t)$. In Fig. 9, the behavior of (8) is plotted for different values of R. For $R = -20$ dB (blue line), a minimum at $n = 12$ is obtained, and after that, the noise increases again. This shows that it is not useful to take more than 12 DPA pulse. With the used low-pass filter (detailed description later) we achieved a reduction R of -36 dB (yellow line). At approximately 50 sense phases, no additional noise reduction is obtained, and therefore, this was used as a maximal phase count.

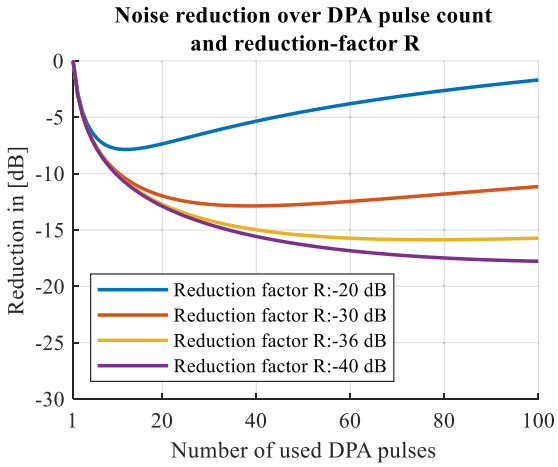

Fig. 9. Theoretical limit of DPA.

IV. Evaluation of Simulated Data

The DPA was analyzed first on simulated data to evaluate noise suppression benefits with the FEM model from Section II. The applied DPA sequence consisted of 50 heat and 50 sense phases with $t_{\mathrm{DPA\_SP}} = 1$ ms followed by a standard TTA sequence with $t_{\mathrm{Heat}} = 3$ s and $t_{\mathrm{Sense}} = 3$ s, which is sufficient to reach the thermal equilibrium for the model. The thermal response was calculated using (7) with a sampling frequency of 10 MHz and is free of noise. A voltage response for a generic semiconductor (a LED with TSP $= -2$ mV/K, $V_f(I_{\mathrm{Sense}}, T_{\mathrm{start}}) = 2.5$ V, and $V_f(I_{\mathrm{Heat}}, T_{\mathrm{start}}) = 2.8$ V) was computed from the thermal response, and white noise was added identical to Section III to reach an SNR of 50 dB compared to the total voltage change during t_{Sense} with (6).

The DPA was applied to the voltage response, as described in Section III. Only the sense phases in t_{DPA} were considered.

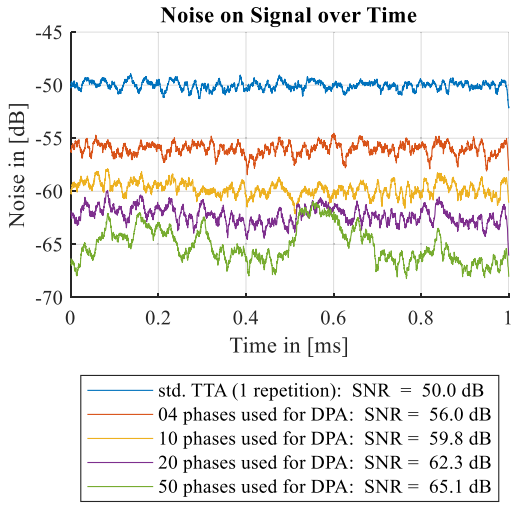

Fig. 10. SNR with DPA until 1 ms.

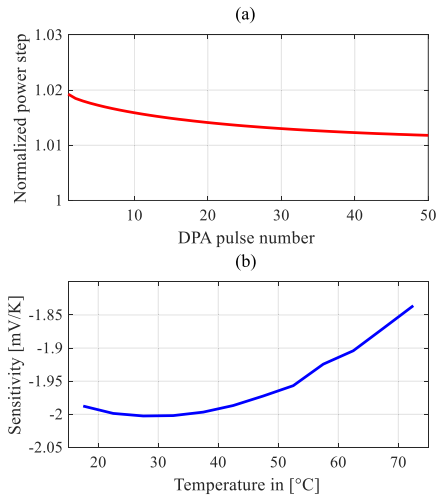

Fig. 11. Correction parameters. (a) DPA power steps normalized to standard TTA power step. (b) Sensitivity over temperature.

For noise suppression on $Z_{\mathrm{th}}(t)$ for $t > t_{\mathrm{DPA\_SP}}$ (for $T_{\mathrm{Off}\,i}(t)$ calculation), different low-pass filters were considered. The best results were achieved using a Savitzky–Golay filter of second order with $f_c = 2$ kHz [23]. The bandwidth of $Z_{\mathrm{th}}(t)$ at 1 ms would be only 0.80 kHz, but f_c was selected higher to avoid signal distortion.

Besides taking all 50 DPA sense phases for averaging, lesser amounts (4, 10, and 20) were also investigated and the results are summarized in Fig. 10. As a reference, the results for the standard TTA sequence with one repetition are included. The SNR for the time $0 < t < t_{\mathrm{DSP\_SP}}$(=1 ms) compared with the noise-free simulated $Z_{\mathrm{th}}(t)$ is shown in the legend of Fig. 10. The plot itself shows a moving SNR over 100 samples. For four DPA phases, the noise is already halved (−6 dB) compared with standard TTA. The SNR further increases with the number of used DPA sense phases, and when using 50 sense phases, the SNR is increased by 15.1 dB. This would be equivalent to averaging over 32 standard TTA repetitions [22, eq. (9.6)]. The DPA sequence would take 6.1 s, while the necessary standard TTA repetitions would need 198 s, which is a time reduction of 97%. The unsteady shape of the green line in Fig. 10 (for 50 sense phases) is caused by not uncorrelated noise addition while $T_{\mathrm{Off}-i}(t)$ calculation but uncritical.

V. Evaluation of Experimental Data

The DPA was tested experimentally after the simulation showed feasibility. The devices under test (DUTs) were white LEDs of type LUXEON F soldered with SAC305 deposited by a 75-μm stencil printing process onto an Al-IMS-PCB. The FEM model used in the previous simulations was calibrated to this setup. Overall, ten LEDs were analyzed with settings identical to the simulation (50 DPA heat and sense phases with 1 ms length and standard TTA with $t_{\mathrm{Heat}} = 3$ s and $t_{\mathrm{Sense}} = 3$ s to reach thermal equilibrium). All measurements were performed on an in-house developed automatic TTA equipment [24] with I_{Heat} set to 1.0 A and I_{Sense} to 20 mA.

A. Correction of Power Step and Sensitivity

The temperature of the junction during DPA sense pulses is smaller than the temperature while sensing in standard TTA. Therefore, for the experimental use of DPA, two parameters of the DUT have to be corrected.

Since the forward voltage of LEDs decreases with rising temperature, the power steps are also decreasing. This change over all DPA pulses is shown Fig. 11(a) where a mismatch between 1% and 2% compared to standard TTA power step is observed. These higher power steps are balanced by correction factors for every DPA response and for every offset $T_{\mathrm{Off}-i}(t)$.

The sensitivity has also to be corrected. For standard TTA, a linear transformation (polynomial of first order) from forward voltage to temperature is used. Since the sensitivity itself drifts slightly with temperature [see Fig. 11(b)], this is not suitable for DPA. For the DUT, a polynomial of third order describes the relation between forward voltage and temperature to good accuracy.

B. Evaluation and Benefit

The measurements showed that $Z_{\mathrm{th}}(t)$ slightly varies over the ten LEDs due to the manufacturing process and material variations. The root cause for this variation is not the target of the investigation and is analyzed in detail in previous papers [5], [17]. Of interest is the comparison of standard TTA and DPA for the same LED. This comparison is shown in Fig. 12 for one LED. The top plot contains four $Z_{\mathrm{th}}(t)$ graphs from 1 μs to 3 s. Two of them were measured with standard TTA (black: one repetition and magenta: ten repetitions). The other two were measured with DPA (blue: 10 DPA phases and green: 50 DPA phases). In the top plot for the whole $Z_{\mathrm{th}}(t)$ time range, all graphs are overlapping and no difference between the four measured $Z_{\mathrm{th}}(t)$ is detectable. To make measurement noise and potential systematic variations visible, the next two plots focus on smaller time intervals. The second plot shows the same graphs, but in the range from 1 μs to 1 ms (whole DPA averaging range) and the third plot from 100 to 200 μs. In these two plots, the curves are overlapping, which shows that DPA also generates the same overall $Z_{\mathrm{th}}(t)$ experimentally as standard TTA. The bottom plot shows the same data and time range as the third plot,

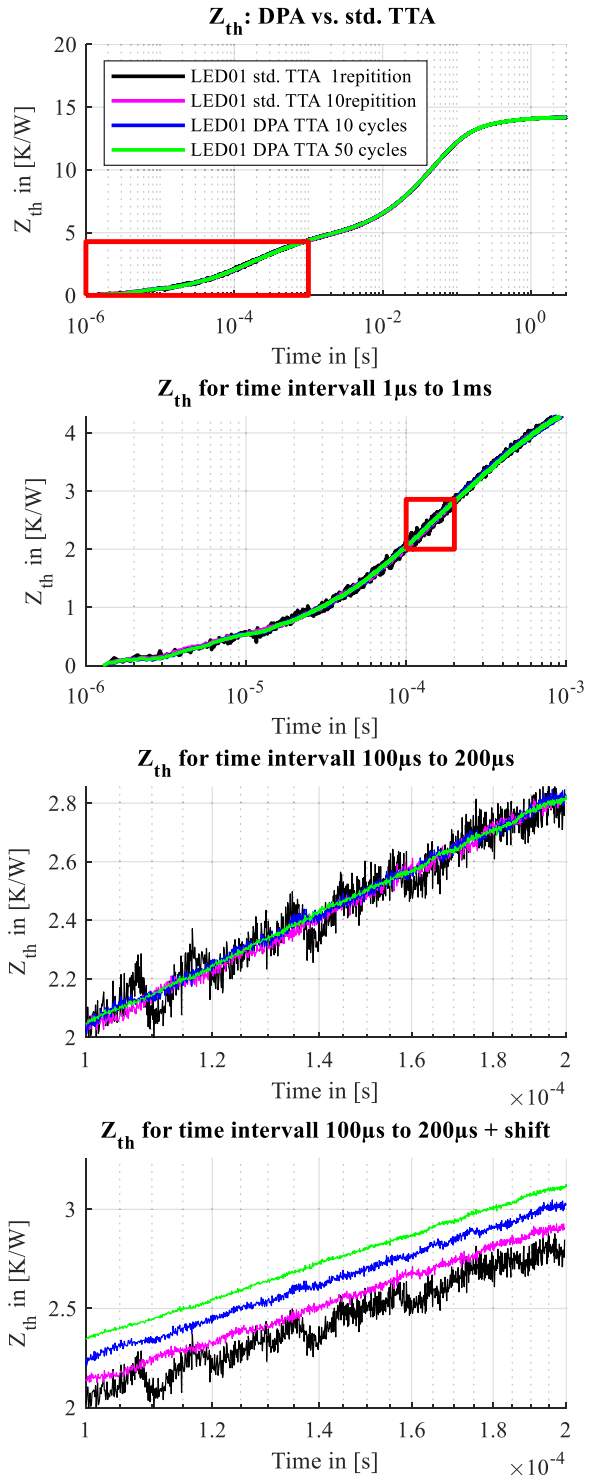

Fig. 12. Experimental results for one LED.

but the curves are shifted apart to make the individual noise behavior easier to see. As expected, the noise on the standard TTA with ten repetitions is reduced compared with standard TTA with only one repetition. The DPA with ten phases shows approximately the same noise as standard TTA with ten repetitions. The lowest noise was achieved by the DPA with 50 phases.

The quantitative verification of the experimental advantages is more complex compared with simulation data since no noise-free signal is available. To compute SNR, two measurements with identical settings on the same LED were subtracted. Assuming that the useful signal is identical, only the noise of the two measurements is left. Since the noise of the two measurements is uncorrelated, it propagates like Gaussian noise, i.e., the noise after subtraction is increased by a factor $\sqrt{2}$ compared to a single measurement. This method is applied to evaluate the SNR for the experimental data. The results are summarized in Table IV for different repetitions in standard TTA and different numbers of used phases in DPA. Included in Table IV is also the necessary measurement time. Standard TTA and DPA start at approximately 50-dB SNR for one repetition and one DPA phase, respectively. The SNR increase is identical for both methods until 16 repetitions or DPA phases, but the required measurement time is basically constant for DPA. A further increase of repetitions in standard TTA would be too time-consuming and was therefore not performed. For DPA, the phase count was raised to a maximum of 50 phases where an SNR of 64.6 dB was achieved. This means an SNR improvement by 14.7 dB, which is close to the simulation results (15.1 dB). Therefore, we have also shown experimental feasibility as one of the benefits of our approach.

TABLE IV
EXPERIMENTAL RESULTS FOR SNR INCREASE

Standard TTA			DPA TTA		
Rep.	SNR	Time	Phases	SNR	Time
1	49.9 dB	6 s	1	49.9 dB	6.002 s
4	55.9 dB	24 s	4	56.0 dB	6.008 s
10	59.9 dB	60 s	10	59.9 dB	6.020 s
16	61.8 dB	96 s	16	61.7 dB	6.032 s
			32	63.7 dB	6.064 s
			50	64.6 dB	6.100 s

VI. CONCLUSION

High SNR is required to evaluate transient thermal data. The three most common evaluation methods were analyzed in this article on their sensitivity to noise. An SNR of approximately 60 dB is necessary for correct application of all three methods. This is difficult to achieve without time-intense averaging over multiple measurements. This is a general challenge for analysis of LTI systems with impulse transfer functions which cause significant response over several decades in the time domain. To improve the SNR for times < 1 ms, this article introduced a new DPA for noise suppression using TTA as an example application. The standard TTA measurement time is only minimally increased by addition of a sequence of short heat/sense phases. The DPA allows averaging over these short intervals by a conversion according to the pulse superposition principle. This article investigated feasibility, limits, and benefits of the DPA on both, simulation and experimental data. An SNR increase of 15.1 dB for simulated data and 14.7 dB for experimental data was achieved by the additional measurement sequence of only 100 ms (50 DPA heat and sense phases with 1 ms length). For the same SNR increase, 30 measurement repetitions would be necessary for

standard TTA for the experimental data. This corresponds to a measurement time reduction of 97%.

REFERENCES

[1] H. Wang, M. Liserre, and F. Blaabjerg, "Toward reliable power electronics: Challenges, design tools, and opportunities," *IEEE Ind. Electron. Mag.*, vol. 7, no. 2, pp. 17–26, Jun. 2013.

[2] J. Broughton, V. Smet, R. R. Tummala, and Y. K. Joshi, "Review of thermal packaging technologies for automotive power electronics for traction purposes," *J. Electron. Packag.*, vol. 140, no. 4, Dec. 2018, Art. no. 40801, doi: 10.1115/1.4040828.

[3] T. Dannerbauer and T. Zahner, "Inline rth control: Fast thermal transient evaluation for high power LEDs," in *Proc. 19th Int. Workshop Thermal Investigations ICs Syst. (THERMINIC)*, Berlin, Germany, Sep. 2013, pp. 172–175.

[4] A. Hanß, "Zuverlässigkeitsuntersuchung von LED-Interconnects mit Hilfe der Transienten Thermischen Analyse," Ph.D. dissertation, Technische Univ. Berlin, Berlin, Germany, 2019.

[5] A. Hanß, M. Schmid, E. Liu, and G. Elger, "Transient thermal analysis as measurement method for IC package structural integrity," *Chin. Phys. B*, vol. 24, no. 6, p. 68105, 2015.

[6] D. Schweitzer, H. Pape, and L. Chen, *Transient Measurement of the Junction-To-Case Thermal Resistance Using Structure Functions*. Zurich, Switzerland: Chances, 2008.

[7] M. Schmid, A. Hanss, S. K. Bhogaraju, and G. Elger, "Time saving averaging algorithm for transient thermal analyses over deterministic pulse superposition," in *Proc. 25th Int. Workshop Thermal Investigations ICs Syst. (THERMINIC)*, Sep. 2019, pp. 1–6.

[8] *Integrated Circuits Thermal Measurement Method - Electrical Test Method*, document JESD51-1, 1995.

[9] *Thermal Impedance Measurements for Vertical Power MOSFETs*, document JESD24-3, 1990.

[10] *Thermal Impedance Measurements for Bipolar Transistors*, document JESD24-4, 1990.

[11] *Thermal Impedance Measurements for Insulated Gate Bipolar Transistors*, document JESD24-6, 1991.

[12] *Thermal Impedance Measurement for Insulated Gate Bipolar Transistors*, document JESD24-12, 2004.

[13] *Implementation of the Electrical Test Method for the Measurement of Real Thermal Resistance and Impedance of Light-Emitting Diodes with Exposed Cooling*, document JESD51-51, 2012.

[14] S. Maximilian and G. Elger, "Measurement of the transient thermal impedance of MOSFETs over the sensitivity of the threshold voltage," in *Proc. 20th Eur. Conf. Power Electron. Appl.*, Riga, Latvia, 2018, p. 1.

[15] V. Székely and T. Van Bien, "Fine structure of heat flow path in semiconductor devices: A measurement and identification method," *Solid-State Electron.*, vol. 31, no. 9, pp. 1363–1368, Sep. 1988.

[16] D. Sundararajan, *Fourier Analysis—A Signal Processing Approach*. Singapore: Springer, 2018, doi: 10.1007/978-981-13-1693-7.

[17] G. Elger *et al.*, "Analysis of solder joint reliability of high power LEDs by transient thermal testing and transient finite element simulations," *Microelectron. J.*, vol. 46, no. 12, pp. 1230–1238, Dec. 2015.

[18] *Transient Dual Interface Test Method for the Measurement of the Thermal Resistance Junction to Case of Semiconductor Devices with Heat Flow Trough a Single Path*, document JESD51-14, 2010.

[19] V. Székely, "A new evaluation method of thermal transient measurement results," *Microelectron. J.*, vol. 28, no. 3, pp. 277–292, Mar. 1997.

[20] T. J. Kennett, W. V. Prestwich, and A. Robertson, "Bayesian deconvolution I: Convergent properties," *Nucl. Instrum. Methods*, vol. 151, nos. 1–2, pp. 285–292, May 1978.

[21] A. Wintrich, U. Nicolai, W. Tursky, and T. Reimann, *Application Manual Power Semiconductors*, 2nd ed. Ilmenau, Germany: ISLE Verlag, 2015.

[22] P. Tagare. (1993). *Signal Averaging*. Accessed: Jul. 31, 2019. [Online]. Available: https://pdfs.semanticscholar.org/5941/95a91dea1a76a6865df707d4e5688f3ed9bc.pdf

[23] R. W. Schafer, "On the frequency-domain properties of Savitzky-Golay filters," in *Proc. Digit. Signal Process. Signal Process. Edu. Meeting (DSP/SPE)*, Sedona, Arizona, USA, Jan. 2011, pp. 4–7.

[24] G. Elger, M. Schmid, A. Hans, and D. Müller, "Automatic panel level transient thermal tester," in *Proc. Symp.*, Bregenz, Austria, Sep. 2017, pp. 594–602

Maximilian Schmid received the M.Sc. degree in electrical engineering from the Technische Hochschule Ingolstadt (THI), Ingolstadt, Germany, in 2014 and 2016, respectively, where he is currently pursuing the Ph.D. degree in microelectronic packaging in cooperation with Technische Universität Berlin, Berlin, Germany.

He is currently an Assistant Researcher with THI.

Sri Krishna Bhogaraju received the M.Eng degree in international automotive engineering from Technische Hochschule Ingolstadt (THI), Ingolstadt, Germany, in 2012, where he is currently pursuing the Ph.D. degree in microelectronics packaging with a focus on copper sintering, in cooperation with Technsiche Universität Berlin, Berlin, Germany.

He was actively involved with ContiTech AG, Hannover, Germany, from 2012 to 2018. He is currently working as a Scientific Research Associate with THI.

Alexander Hanss received the M.Sc. degree in electrical engineering from the Hochschule München, Munich, Germany, in 2013, and the Ph.D. degree in microelectronic packaging and LED reliability from Technsiche Universität Berlin, Berlin, Germany, in 2019.

Then, he worked as a Scientific Research Associate with the Technische Hochschule Ingolstadt (THI), Ingolstadt, Germany.

Gordon Elger received the Diploma degree in physics and the Ph.D. degree from the Free University of Berlin, Berlin, Germany, in 1994 and 1998, respectively.

Afterward, he worked at Fraunhofer IZM, Berlin, Hymite, Berlin, Germany, Electrolux, Prodenone, Italy, and Royal Philips, Aachen, Germany, in the field of microelectronics packaging. Since 2013, he has been a Professor for manufacturing technologies of electronics at the Technische Hochschule Ingolstadt, Ingolstadt, Germany.